NEW METHOD FOR SURFACE PRESSURE MEASUREMENTS

Sergey D. Fonov[*], Larry P. Goss[†], E. Grant Jones[‡], Jim W. Crafton[§], Vladimir S. Fonov[**]
Innovative Scientific Solutions, Dayton, OH
Michael Ol[††]
Wright Patterson AFRL, Dayton, OH

New method and means for measuring the pressure of fluid on an aerodynamic surface, based on measurements of three-dimensional elastic deformations of a polymeric film is disclosed. Object is coated by elastic polymeric film with known shear module. Calibration is accomplished by measuring of the polymeric film deformation under action of locally applied force and calculating of a response function field based on local 3D deformation measurement and polymeric film thickness distribution. Surface pressure and shear tension fields are calculated using response functions and film deformation field. Method provides significant improvement of sensitivity and time response relative pressure sensitive paint based on oxygen quenching phenomena. The first experimental results obtained in water and air flow environments with flow velocity 0.3 – 0.4m/s (water) and 10 - 20m/s (air) are presented and discussed.

Nomenclature

Ω - 3D (2D) volume of elastic material
Γ - Boundary of Ω
u, v, w – displacements
ε - strains
σ - stresses
λ, μ - Lame constants, μ - shear modulus
E – modulus of elasticity
ν - Poisson ratio
Λ - film thickness
g, G – impulse response matrix
n, s – normal and tangential components of impulse matrix
L – vector of surface stresses
R – vector of surface deformations
ρ - polymer density
f_o - elastic layer natural frequency (first shift deformation tone)
a, b, k, t – approximation coefficients

I. Background

Convenient, reliable and inexpensive methods for determining pressure maps of surfaces, particularly aerodynamic objects, are under development up to now. Standard approach is using pressure taps, which are drilled into the surface under study and connected via tubing to the multiplexed pressure gages or pressure gage arrays.

---

[*] Senior Scientist, 2766 Indian Ripple Road, Dayton, OH 45440-3638 sfonov@innssi.com, www.innssi.com/psp

[†] ISSI President, 2766 Indian Ripple Road, Dayton, OH 45440-3638

[‡] Senior Chemist, 2766 Indian Ripple Road, Dayton, OH 45440-3638

[§] Scientist, 2766 Indian Ripple Road, Dayton, OH 45440-3638

[**] Scientist, 2766 Indian Ripple Road, Dayton, OH 45440-3638

[††] Senior Scientist, AFRL, Dayton, OH

Hundreds pressure taps are required to get pressure distribution on the total surface but due to significant distance between taps additional sophisticated interpolation procedures are required usually [1]. Pressure taps provide information only about static or normal pressure component acting on the surface. Tangential pressure components or shear stresses should be measured as well and up to now these components are measured or by non-direct approach using for example heat flux measurement or by miniature balance system imbedded into model surface and measuring shear force acting on floated peace of a model surface [2,3].

In 1980, Peterson and Fitzgerald proposed oxygen quenching of fluorescent dyes for flow visualization [4]. Similar approach was patented by Pervushin and Nevsky [5]. Since this time many efforts were applied to develop this approach to the reliable and quantitative Pressure Sensitive Paint (PSP) measurement technique [6]. PSP is based on oxygen quenching of the molecular photoluminescence. Surface under study is covered by thin layer of a polymer with embedded luminophore molecules. Oxygen from the ambient flow can diffuse in polymeric layer and its concentration in the layer is proportional to static air pressure on the upper layer surface. Appropriate light source excites luminescence which local output due to oxygen quenching is function of local oxygen concentration and as mention above static air pressure on the upper layer surface [7].

Oxygen diffusion in PSP layer determines mainly PSP response time to pressure change on the upper surface [8]. This time can be estimated as $\tau \approx \Lambda^2/D$, where Λ is PSP layer thickness and D – oxygen diffusion coefficient. For practically ultimate layer thickness about 1-2 micrometers response time is about 2 - 4 ms that apply upper boundary for PSP applications for investigation of the transient phenomena in the air flow.

Normalized Luminescence output function I/Io at some local point R on the layer surface can be approximated by (Figure 1):

$$I/Io=1/[(A(T)+B(T)P] \qquad (1)$$

where Io – output at P=0.0, A(T) and B(T) are function of the local layer temperature T and P is static pressure
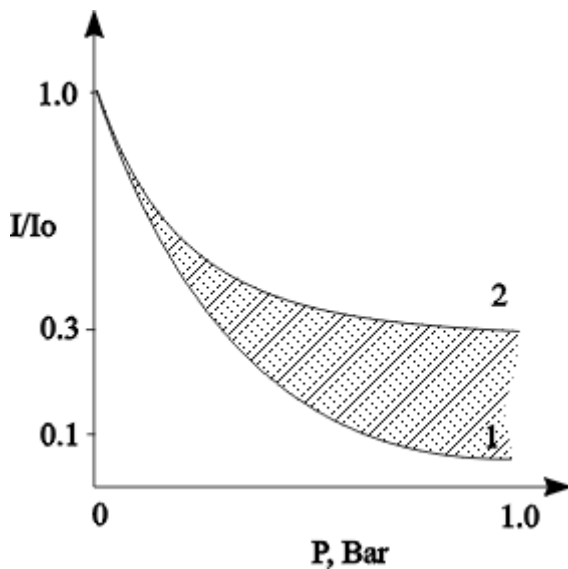

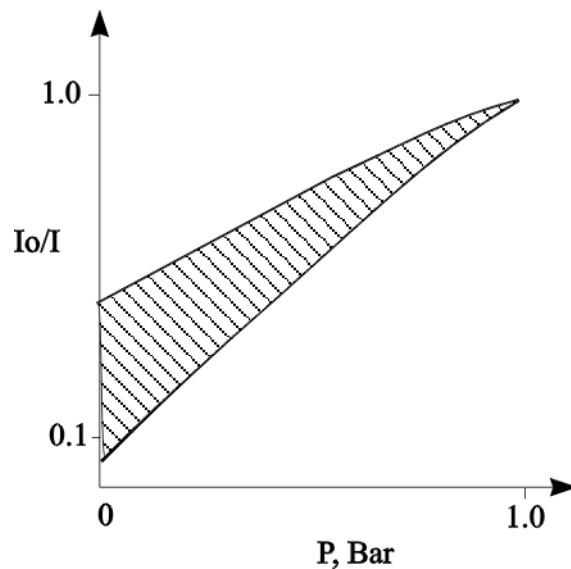Figure 1. Relative intensity as function of pressure   Figure 2. Stern-Vormer approximation of PSP signal

PSP based on the oxygen quenching is essentially absolute pressure gage, and all practically workable formulations are located between curve 1 and 2. PSP sensitivity dI/dP is function of the pressure level dramatically decreasing as $1/P^2$ that implies additional problems. Pressure dependence can be linearized using Stern-Former approximation:

$$Ir(P,T)=Io/I = A(T)+B(T)*P \qquad (2)$$

Typical function of inversely normalized intensity Ir(P,T) is presented at Figure 2. Sensitivity dIr/dP for most currently available PSP formulation varies in the range $(0.5 -1.0)*10^{-3}$%/Pa and can not be increased significantly due to physical and photochemical properties of available formulations what creates problems for PSP

applications where pressure variations are small. Typical example is pressure field measurements at low subsonic velocities – Mach number below 0.05. Pressure variation on the model is proportional to squared Mach number. It means that pressure variation range δP for Ma=0.05 (V=35mile/h) is about 100Pa that is hundred time less then at M=0.5 (V=350mile/h and δP=10^4Pa) but PSP sensitivity can't be modified in the such scale and only one possibility to get reliable result is increasing of the signal to noise ratio in the acquired information (usually images) and compensating all disturbing factors like illumination non-stability, model displacement and deformation, temperature effects. PSP temperature sensitivity varies between 100Pa/^{o}C to 1000Pa/^{o}C that is comparable with total pressure variation range for Ma=0.05. Finally PSP measurements at flow velocities below Ma=0.05 are semi-quantitative up to now and require significant efforts.
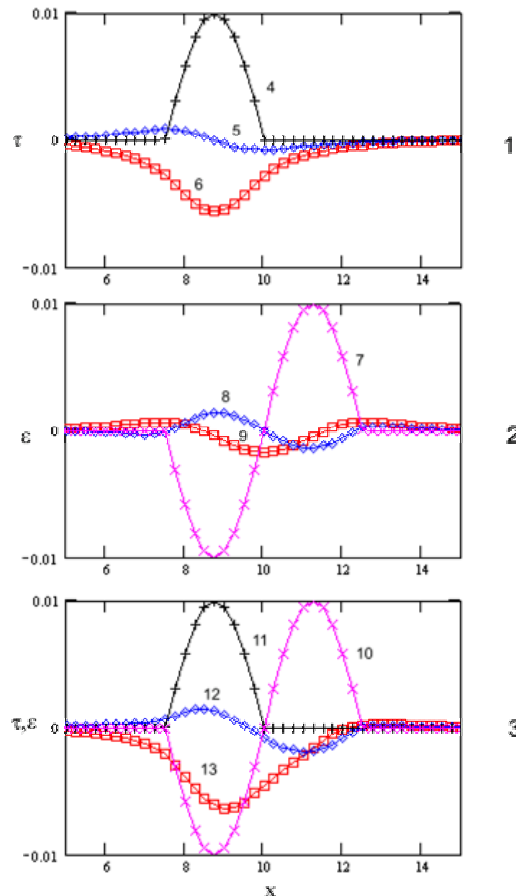

Figure 3 FEA of action of shear force (Plot 1), normal force (Plot 2) and their combination (Plot 3)

Mapping of the shear stresses is accomplished up to now on the semi-quantitative level using liquid crystals [9] or different approaches with oil film measurements [10]. .At the beginning of nineties method for direct measurements of surface shear force was offered [11, 12]. Method includes mount on the model surface of sensing element in the form of film made of flexible material-polymer gel of desired thickness with known shear modulus; markers are applied to film and model surfaces, and shear deformation of film caused by flow is measured by interference method; shearing stress is determined using Hooke's law for shear strain. Markers may be made in the form of reflection grating placed on model surface(under film) and transmitting grating on film surface enabling use of moiré phenomenon for recording shear strain. Method provides improved accuracy and informative capacity due to determining local values of shearing stress. The main drawback of this method is connected with the fact that gradients of the normal pressure creates shear displacement of polymer gel as well and method will work well only in the absence of normal pressure gradients. This is demonstrated by results of Finite Elements Analysis presented in Figure 3, cases 1, 2 and 3.

Case 1. Shear force 4 with amplitude 100Pa which is applied at the surface of polymer gel having thickness 1mm, shear module μ=600Pa and Poisson ratio ν=0.496, creates shear deformation 6 accompanied by normal deformation 5 (referred to gel thickness 1mm)

Case 2. The same layer under action of the normal pressure distribution 7 having amplitude 100Pa. Shear and normal deformations are presented as distributions 9 and 8.

Case 3. Combination of loads from cases 1 and 2. Shear deformation 13 is determined by joint action of normal and shear forces and calculation of the shear force distribution will require information about normal force as well. It is worth mentioned that normal deformations are less sensitive to the shear force action. Practically interesting cases in flow investigations are characterized by regions with large pressure pikes and pressure gradients but usually shear forces and shear force gradients are 10…100 smaller that creates more difficult problem for recognition of input in shear deformation from normal and shear surface load components.

II. New approach

The main goal of the present work was to provide method for measuring the static pressure of fluids on a surface, which do not suffer from drawbacks of the pressure sensitive paints based on oxygen-quenching, like necessity of the quencher in fluid, fluid compressibility, limited pressure sensitivity and frequency response.
It is the second goal was to provide method for measuring the shear stress of fluids on a surface, which can work in combination with normal pressure measurement and provides possibility to resolve normal and shear tension components. Both goals should be supported by method and means for direct calibration.

Standard approach to reach high measurement accuracy is increasing of the gage sensitivity with measuring only increments relative some etalon value located in measurement range – using for example differential pressure gage instead of absolute pressure gage. This is idea of differential pressure measurement is cornerstone of this method. Polymer behaves like non-compressible fluid but contrary standard fluid tries to recover original shape after removal of deformation force.
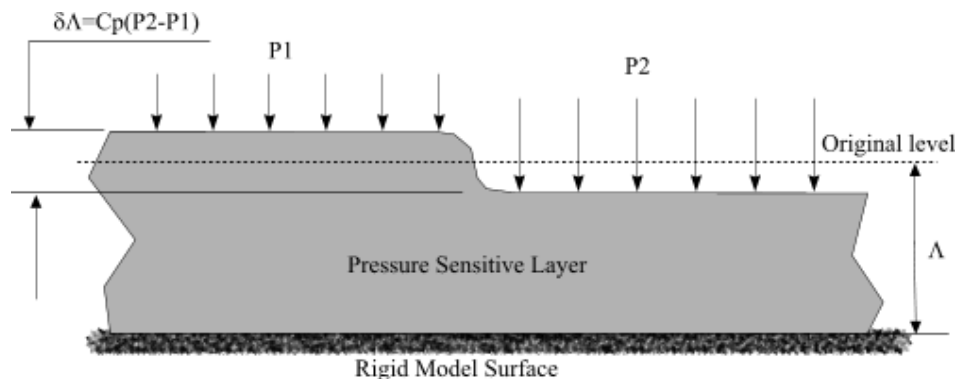

Figure 4 Realization of the Differential Principle

Pressure loads P1 and P2 applied at adjacent surfaces will displace polymer material that resulted in change of the local layer thickness at value δΛ ~ Cp(P2-P1). This is only crude scheme; in general deformations of the polymeric layer are governed by pressure gradients and shear force as well.

Range of linear frequency response of S3F is limited by natural frequency of shear oscillation and can be estimated as

$$f_0 = \frac{1}{2\pi}\sqrt{\frac{\mu}{\rho\Lambda^2}}$$

Changing μ∈(100…1000)Pa, and Λ∈(0.1..1)mm it is possible to adjust frequency response in the range 0.3..10KHz that is approximately 100 times better than standard PSP based on oxygen quenching.
In order for a pressure sensitive film to produce desired results it must be applied on the surface under study. There are several ways for film applications like airbrush spraying and "shrink-fit method". The last provides films with controlled thickness and useful for evaluation phase. Source components are poured into flat cavity having smoothed or even polished bottom. After polymerization the film is pealed of and placed on an airfoil. Film

thickness can be estimated by direct measurements using for example optical absorption or capacitor type thickness gage. The next step is the film calibration. This procedure includes application of specified load on the film surface and measurements corresponding normal and tangential deformation distribution – evaluation of the film response functions. The smaller load application area the more film response function will corresponds to impulse function.

Consider for simplicity a 1D load application. In this case deformations can be treated in 2D space. Plate has a cavity with a rectangular cross-section [0,20]x[0,1] The cavity is filled with S3F and the characteristic length (d=1 mm) is the thickness of the S3F. Concentrated constant loads (normal or tangential) are applied on the interval [9.9, 10.1]. Zero deformations on the cavity walls determine boundary conditions for this problem.

The S3F is an elastic solid and is deformed under the applied forces. A point in the solid, originally at (x,y) goes to (X,Y) upon application of the load. If the displacement vector $\vec{r} = (r_1, r_2) = (X - x, Y - y)$ is small, Hooke's law relates the stress tensor σ inside the solids to the deformation tensor ε [13]:

$$\sigma_{ij} = \lambda \delta_{ij} \nabla . \vec{r} + \mu \varepsilon_{ij}, \quad \varepsilon_{ij} = \frac{1}{2}\left(\frac{\partial r_i}{\partial x_j} + \frac{\partial r_j}{\partial x_i} \right) \qquad (3)$$

where δ_{ij} is the Kronecker symbol ($\delta_{ij} =1$, if i=j, $\delta_{ij} =0$, if i≠j), and λ, μ are two Lame constants describing the material mechanical properties in terms of the modulus of elasticity E, and Poisson ratio ν as:

$$\lambda = \frac{E\nu}{(1+\nu)(1-2\nu)}, \quad \mu = \frac{E}{(1+2\nu)} .$$

The equation of elasticity are written in variation form for the displacement vector $\vec{r}(x) \in \Omega$ as

$$\int_{\Omega}\left[\mu \varepsilon_{ij}\left(\vec{r}\right)\varepsilon_{ij}\left(\vec{w}\right) + \lambda \varepsilon_{ii}\left(\vec{r}\right)\varepsilon_{jj}\left(\vec{w}\right)\right] = \int_{\Gamma}\vec{\tau} \cdot \vec{w}, \quad \forall \vec{w} \in \Omega \qquad (4)$$

and the integrals are in volume Ω or on volume boundary Γ [14]

Solution results are presented at Figure 5. Zoomed view of the deformed grid shows that deformations concentrated mainly in region with diameter about 2..3 thickness of the elastic layer.
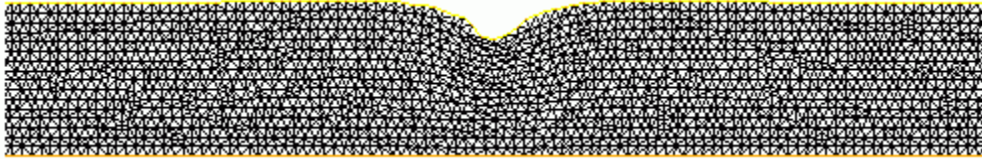

Figure 5 Solution of the problem (Zoomed view of the deformed FE grid)

Plots on Figure 6 present normal (blue line) and tangential (red line) displacements as result of action of the rectangular pulse load (pink line) on the layer surface. Magnitude of tangential displacement approximately two times more then magnitude of normal displacement on the region outside of applied load. So, information about tangential displacement can be used for normal force visualization as well. Of course normal displacements below load application region are significantly larger. This function of normal displacement distribution $g(x)$ can be treated as reaction on the pulse load $\delta(x)$. Next assumption will be that elastic reaction $\mathbf{R}(x) \equiv (R_x, R_y)$ on the arbitrary surface load $\mathbf{L}(x)=(L_x, L_y)$ can treated as linear system:

$$\mathbf{R}(x) = \int \mathbf{G}(x - x')\mathbf{L}(x')dx' \qquad (5)$$

Normal displacement reaction on action of the normal "pulse" force (Fig. 6) can be approximated by function:

$$\tilde{n}_n(x) = \begin{bmatrix} 1 \\ \exp(-|x|/k1) \\ \exp(-|x|/k2) \end{bmatrix} \cdot \begin{bmatrix} a_0 & a_1 & a_2 \end{bmatrix}, \text{ where parameters } (k1, k2 \text{ and } a_i \text{ are obtained to minimize}$$

approximation error. Shear displacement reaction on action of normal "pulse" force is approximated by function

$$\tilde{n}_s(x) = \begin{bmatrix} 1 \\ x\exp(-|x|/k3) \end{bmatrix} \cdot \begin{bmatrix} a_3 & a_4 \end{bmatrix}.$$
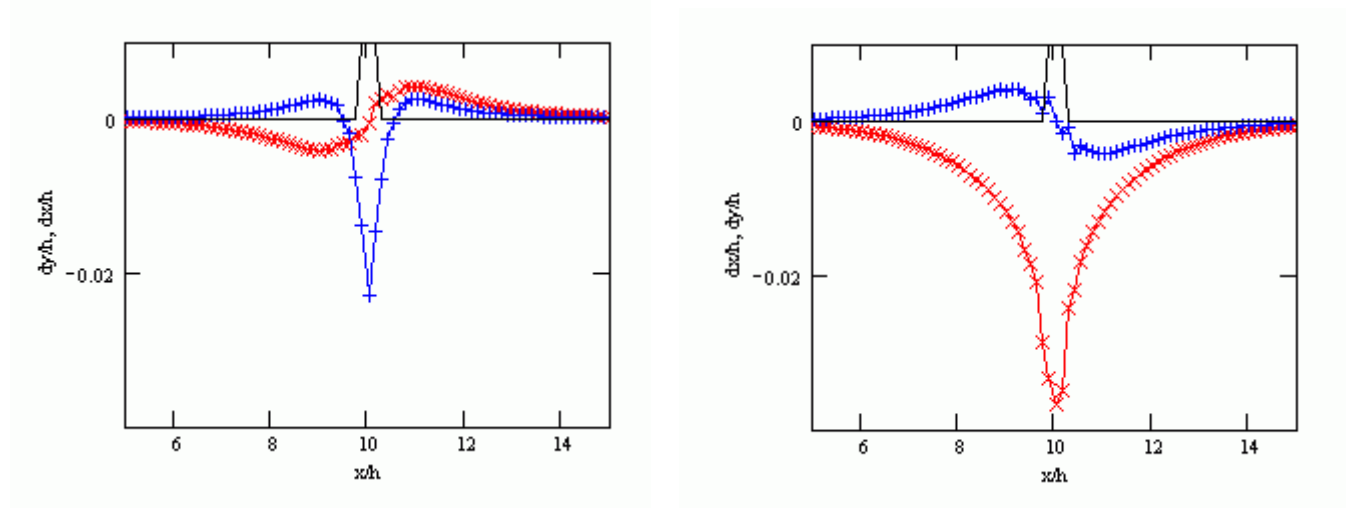

Figure 6 Displacements on the upper boundary, right plot -normal load, left plot – shear load 10 Pa, layer thickness h=1mm, E=600, v=0.495, (tangential displacement– red line, normal displacement – blue line, load distribution – black line).

Similarly for case of shear "pulse" load, approximations for normal $\tilde{s}_n$ and shear $\tilde{s}_s$ reaction can be presented as:

$$\tilde{s}_n(x) = \begin{bmatrix} 1 \\ x\exp(-|x|/t1) \end{bmatrix} \cdot \begin{bmatrix} b_1 & b_2 \end{bmatrix},$$

$$\tilde{s}_s(x) = \begin{bmatrix} 1 \\ \exp(-|x|/t2) \\ \exp(-|x|/t2) \end{bmatrix} \cdot \begin{bmatrix} b_3 & b_4 & b_5 \end{bmatrix}.$$

Reaction on the arbitrary load $L_j = (L_{nj}, L_{sj})$ applied at the interval $[x_0, x_N]$ can be presented as:

$$R_{nj} = \sum_{k=0}^{N} L_{nk}\tilde{n}_n(x_j - x_k) + L_{gk}\tilde{s}_n(x_j - x_k) \tag{6}$$

$$R_{sj} = \sum_{k=0}^{N} L_{nk}\tilde{n}_s(x_j - x_k) + L_{gk}\tilde{s}_s(x_j - x_k)$$

This system of linear equations (2) relative unknown L_k has diagonally dominant matrix (Figure 7)

$$\mathbf{G}_{jk} = 1/\mu \begin{pmatrix} \tilde{n}_{njk} & \tilde{s}_{njk} \\ \tilde{n}_{sjk} & \tilde{s}_{sjk} \end{pmatrix}, \text{ which can be inverted and solution of linear equations can be written as:}$$

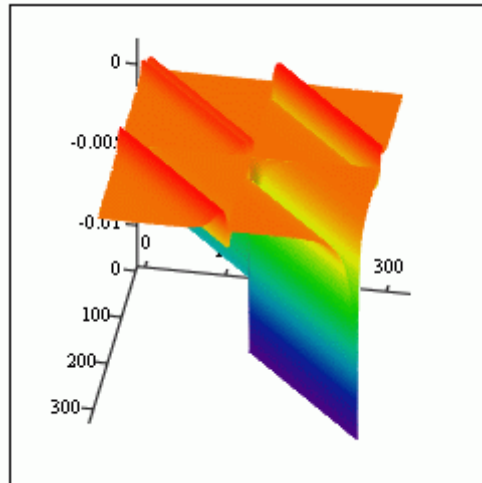$$\mathbf{L} = \mathbf{G}^{-1} \cdot \mathbf{R} \tag{7}$$

Figure 7. 3D presentation of G matrix

To visualize effectiveness of such approach reconstruction of cosine type load was considered. Results are presented at Fig. 8. Normal load distribution

$$L_y(x) = (1 + \sin(2\pi(x-10)/D) \quad x \in [10 - D/2; 10], \quad D = 5.0$$

and tangential

$$L(x) = (1 + \sin(2\pi(x-10)/D) \quad x \in [10 - D/2; 10 + D/2], \quad D = 5.0$$

were used as input for FEA, resulting displacement were used in equation 7 with matrix $\mathbf{G}^{-1}$ taken from above presented estimation for pulse loads.

Average error between applied and recovered load is less then 1% on the load application interval and grows up 3% outside this interval. It means that smooth loads can be recovered with acceptable for such simple model accuracy.

Response functions depend on film thickness. Plots on Figure 9 present results of FEA modeling of response on harmonic normal and tangential loads applied on interval d on S3F with thickness d1. Maximum deformations as function of d1/d can be treated as measure of spatial Amplitude-Frequency Characteristics of S3F. AFC for normal load (red line) and tangential load are quite different especially at low d1/d – low spatial frequency that provide possibility to adjust sensitivity for pressure and shear force measurements.
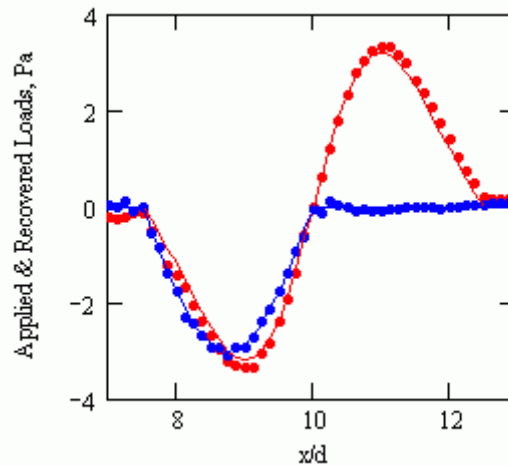

Figure 8. Reconstruction (points) of the applied surface loads (blue line– normal, red line– tangential)
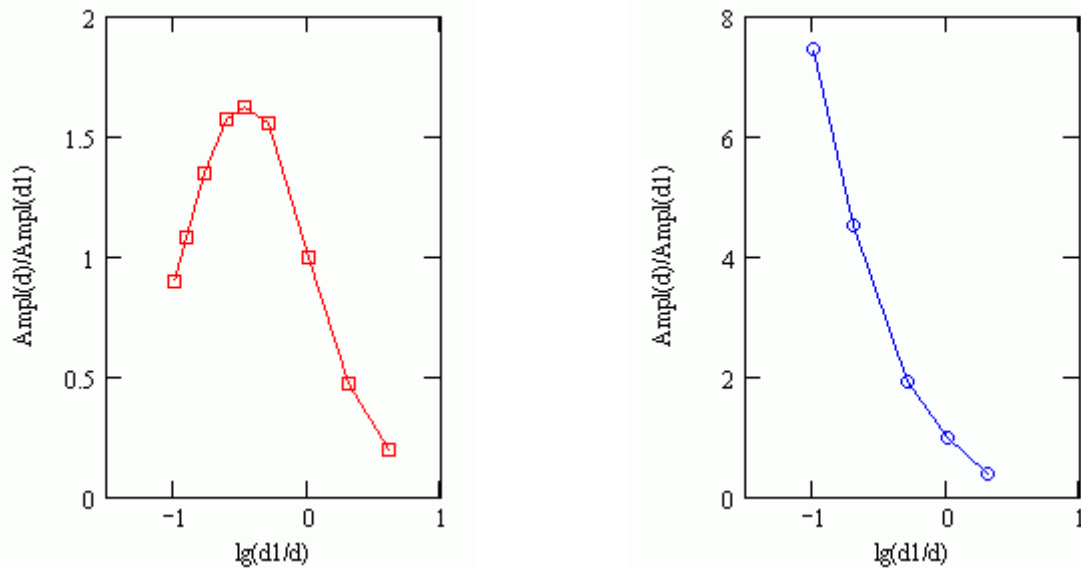
Figure 9. Estimation of AFC for normal (left) and tangential (right) loads

Shear displacements can be measured by comparison of two images of marker pattern applied on the upper surface of pressure sensitive paint. Additional marker pattern applied on the substrate can be used for image registering before their rationing and compensation of model movement and deformation under action of aerodynamic or inertia forces. Cross-correlation procedure applied for two images with markers patterns provides 2D shear displacement field. Cross-correlation function is calculated in 2D window sequentially step by step scanning total surface of images. Window dimensions are determined by marker density and minimum scale of shear field. Steps are about half-size of window dimension to exclude over-sampling. Normal deformations can be measured using for example variation of luminescent signal from luminophore dissolved in S3F. Due to low compressibility of S3F luminescence output for optically transparent film will be proportional to the local film thickness. This approach in combination with marker pattern provides possibility to acquire all three components of deformation vector from comparison of wind-of and wind-on images. S3F sensitivity should be adjusted in accordance with dynamic range of surface forces taking into account limitation on maximum acceptable deformation of the surface under study due to possible influence on the flow itself. Usually relative normal deformations are below 1-2% (referred to the film thickness), film thickness is less then 1-10% of characteristic thickness of the model.

III. Experimental Examples

Shear Stress Module and film thickness are the main parameters determining sensitivity and spatial resolution of the S3F. Shear module µ can be measured directly by applying shear force to the film with known thickness and measuring corresponding displacement. Response functions can be estimated using FEA model described before but some efforts were applied to verify FEA model itself.

Practically it is possible to create stable PSF having shear stress module in the range $\mu= 30….3000Pa$ and more. Plots on Fig.10 demonstrate calibration curve for practical S3F compositions. Composition have good linearity and small hysteresis, which is in the range of tangential displacement measurement accuracy $\sigma=0.1-0.3\mu m$. Total linear dynamic range of the displacement is about 1000µm that is large enough compared with S3F layer thickness 1730µm for this case.
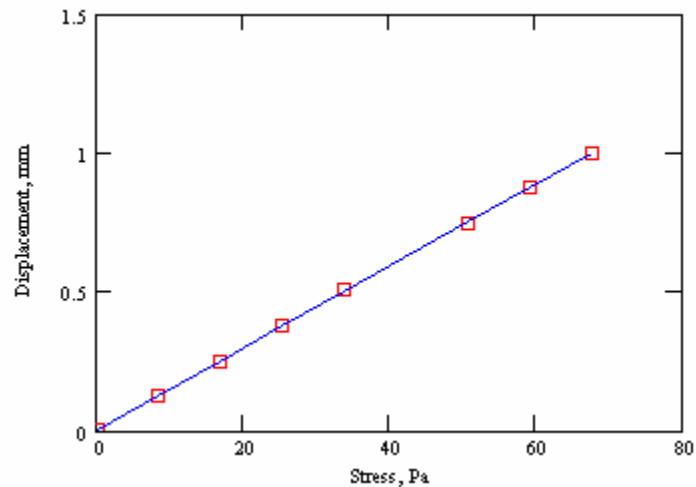
Figure 10. Calibration curve for S3F composition with shear stress module μ=117Pa

Typical measurement setup for S3F application is presented in Figure 11. All three deformation components can be extracted from wind-of, wind-on images taken by one hi-resolution CCD camera. Normal component in this configuration is measured using luminescence signal from S3F. It requires stable light source and at least 12-bit amplitude resolution. Dynamic measurements usually require pulsed light sources and reference channel to compensate exposure non stability and model displacements. Good approach in this case is using color CCD camera like Hamamatsu C7780 having 3 CCD chips for R, G and B channels. Reference signal in green region is created by luminescence from S3F substrate, information about normal deformation is acquired in red region and information about shear deformations is taken from blue region. Static measurements were conducted mainly using QIMAGING RETIGA EX monochrome CCD camera having 1280 by 1024 spatial resolution and 12-bit amplitude resolution in combination with ISSI LED lamps (output in 406nm or 460nm).
OMS 3.1 software package was used for image processing which include image alignment, normalizing, and calculation of the shear displacement fields. Software provides model displacement compensation as a rigid body using additional information from markers located on S3F substrate. Output results are saved in TecPlot data format.
    The first try to use S3F for pressure field visualization demonstrated very promising results. Successful visualizations were conducted for flow velocity from parts of m/s to 1m/s (in water), and from 10m/s to 45m/s in air flow.
    Simple models with known pressure and friction force distributions were used for the feasibility tests. One of such models is presented at Figure 12. This is plate having wedged leading edge installed vertically at test section floor at zero side angle. Plate has cavity near by leading edge filled with S3F. Flow velocity varied from 10 to 20m/s. Normal and shear deformation fields obtained at 20m/s are presented at Figures 13 and 14.
Deformation field in the center line section can be considered as two dimensional and data recovery scheme described above can be used for this case. Plots (Figure 15) show comparison of measured pressure and friction force coefficients with CFD estimations.
    Delta wing model (Figure 16) was tested at flow velocity range 5- 40m/s, angle of attack 10°. Upper surface has cavity filled with S3F with the thickness 1mm. Fine powder was applied on the upper surface of PSF to create pattern for shear deformation measurements.
Field of the relative thickness distribution is presented at Figure 17. Vortex above wing surface creates narrow decompression region with pressure gradient oriented mainly across the ambient flow direction, so for each cross section elastic deformation problem can be treated as plane. Cross-correlation technique provided evaluation of the shear displacement field presented at Figure 18. Vertical component of shear displacement vector presented in false color bears information about local shear force distribution under vortex flow.
Figures 20 and 21 are presented to compare sensitivity of standard PSP based on oxygen quenching and PSF for approximately identical flow conditions. PSF sensitivity is about 25 times more and comparable SNR on the resulting image can be obtained by acquisition only 3 images instead of about 180 images for standard PSP.
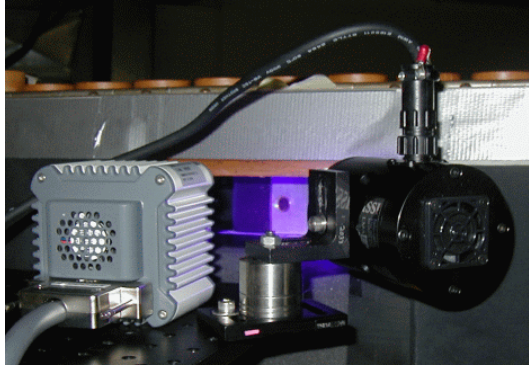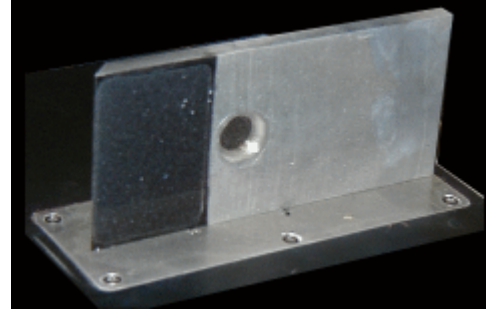
Figure 11. Typical experimental setup

**Figure 12. Tested model. Cavity having depth 1mm
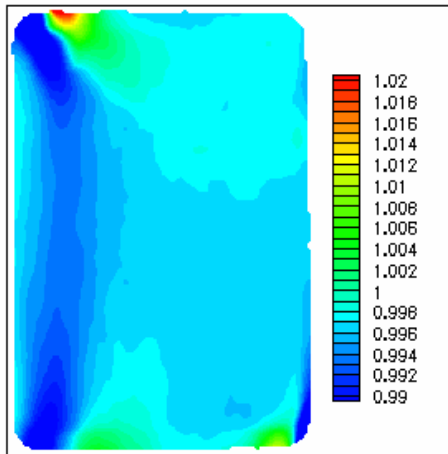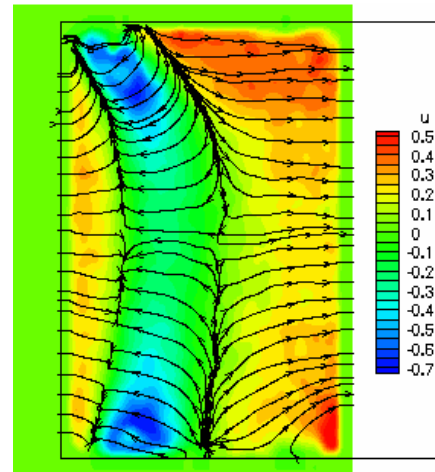(front black part is filled with S3F)**

Figure 13. Normal deformation field

Figure 14. Shear deformation field.

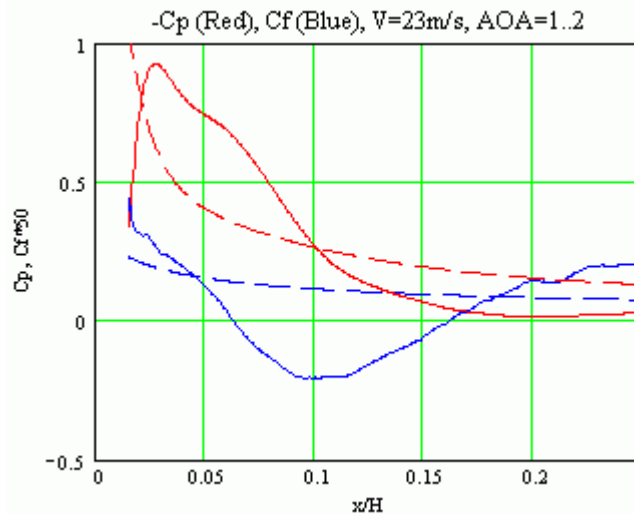**Figure 15. Reconstructed -Cp (red) and Cf*50 (blue) distributions
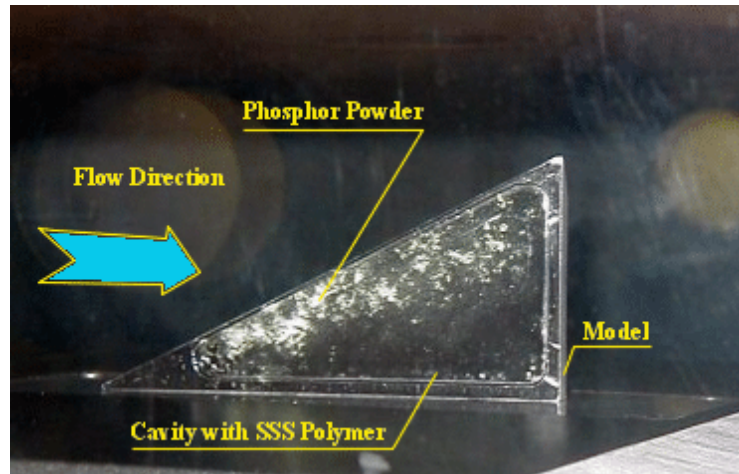compared with CFD (2D potential flow) and Blasius estimations (dashed lines),V=23m/s**
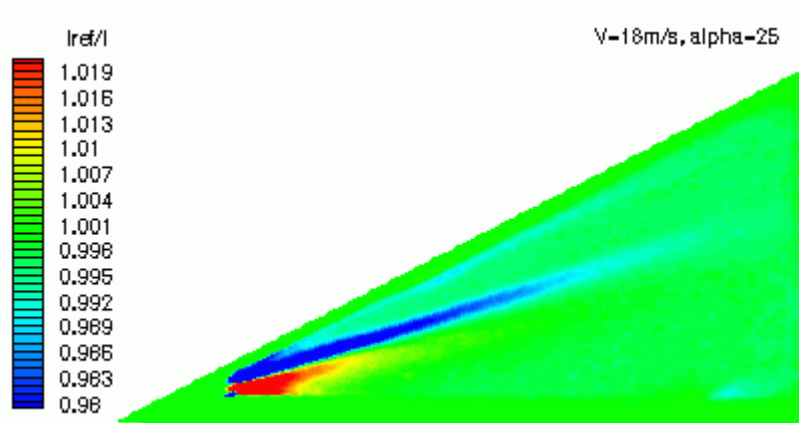
Figure 16 Delta wing model

Figure 17 Relative thickness distribution on the surface of the delta wing model. Flow velocity 18m/s, angle of attack 12°.
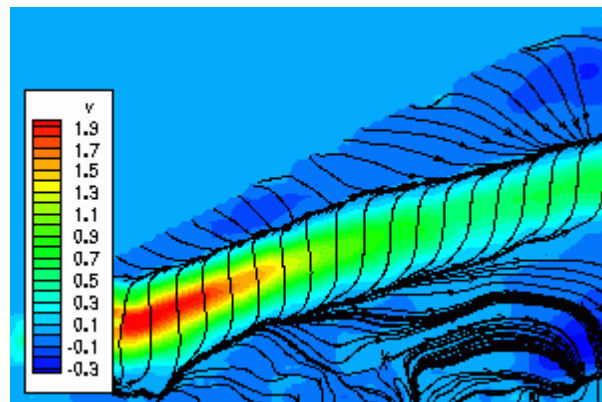

Figure 18 Shear Displacement Vector Field and vertical component of shear vector (expressed in pixels - false color presentation) on the surface of the delta wing model. Flow velocity 18m/s, angle of attack 12°
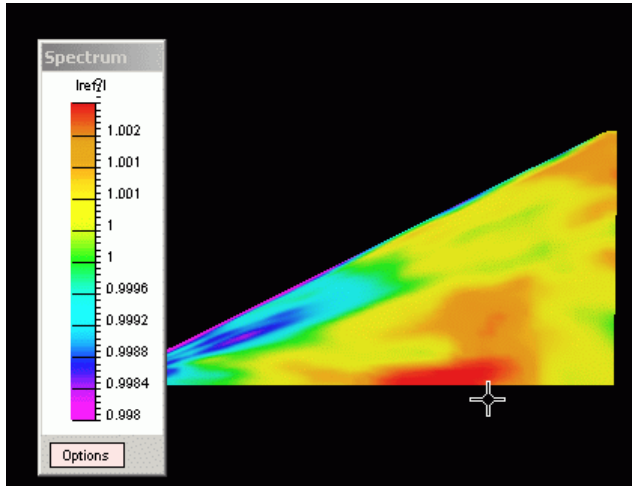
Figure 19. Fib based PSP, V=12m/s, angle of attack 15°, relative intensity field.Total variation of the intensity is about 0.4%. Field was obtained after averaging of 64 images for each of wind-off, wind-on and dark conditions. Adaptive Gauss filter with effective aperture 5 nods was applied.
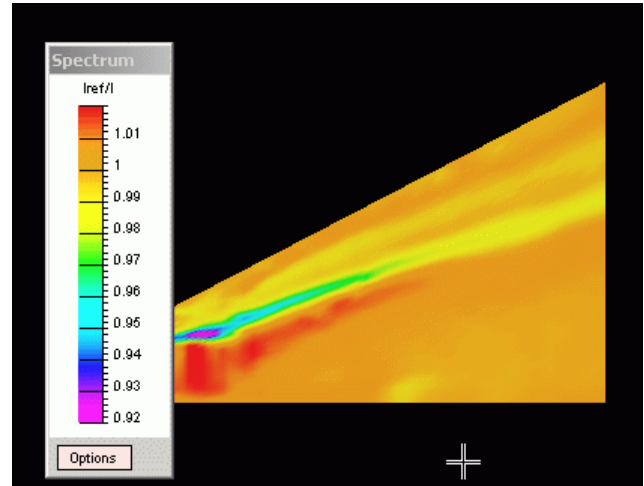

Figure 20 S3F results, V=16m/s, angle of attack 10°, relative intensity field. Total variation of the intensity is about 10%. Field was obtained using single images for wind-off, wind-on and dark conditions. Adaptive spatial filtering was applied with Gauss aperture having effective diameter 5 nods.

Pressure Distribution Measurements on the models immersed in the water can be the most attractive application field for S3F due to fact that standard PSPs do not work in the absence of the oxygen and very low compressibility of the water itself. Regular measurements with S3F were initiated in WP AFRT water tunnel. The first model was double delta wing presented in Figure 21. S3F was created in cavity having thickness 1.5mm. Shear module was in the range 30 – 60Pa, that in combination with spatial resolution of 3D deformation measurements about 1um, provides resolution in pressure and shear force measurements about 0.1- 0.2 Pa.
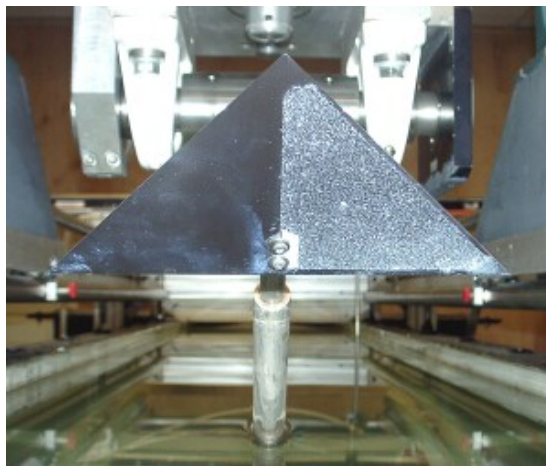

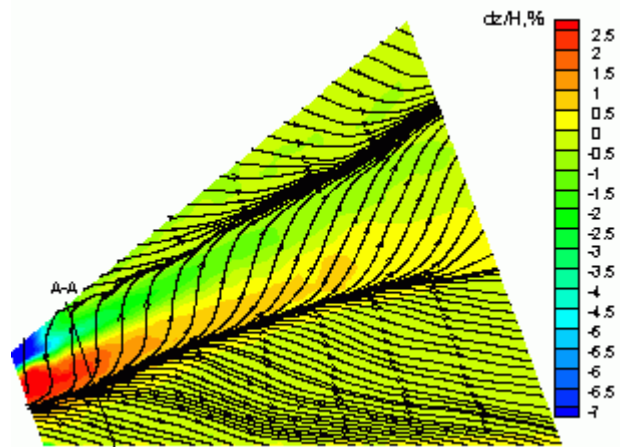**Figure 21. Delta Wing Model with S3F created in cavity (right side)**

Figure 22. Shear force visualization on Delta Wing Model (angle of attack 15°, water flow velocity 0.4 m/s) Normal deformation field is presented in false color.

Figure 22 presents streamlines of the shear displacement field and normal deformation field (false color). Pressure and shear force distributions in the section A-A are shown at Figure 23.
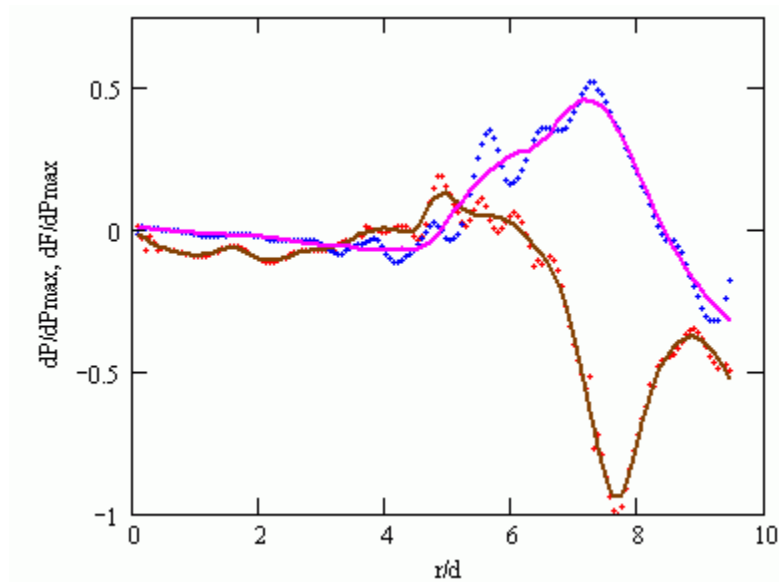
Figure 23 Reconstruction of pressure (red) and shear (magenta) distributions in section A-A

IV. Conclusions

Feasibility of S3F for pressure and shear force measurements is demonstrated. Future development connected mainly with data processing algorithms is required. The final goal is S3F application for 3D loads on the models with a complex shape.

References

1. Jewel B. Barlow, William H. Rae, Alan Pope, "Low-Speed Wind Tunnel Testing", Wiley, John & Sons, Inc., 1999, 800pp.
2. Magill et al., "Study of a Direct Measuring Skin Friction Gage with Rubber Compounds for Damping", AIAA Paper 2000-2395).
3. J.W. Naughton, M. Sheplak "Modern Development in Shear Stress Measurement", Progress in Aerospace Sciences 38(2002) 515-570
4. Peterson, J.I. et al., "New Technique of Surface Flow Visualization Based on Oxygen Quenching of Fluorescence", Rev. Sci. Instrum. 51(5):670-671, 1980
5. Nevsky, L.B.; Pervushin, G.E. "Method of pressure distribution measurement with the indicating coating" Patent SU 1065452/1981
6. Bell James H et al. "Surface Pressure Measurements Using Luminescence Coatings" Annual Rev. Fluid Mech. 2001. 33:155-206.
7. Mosharov V, Radchenko V, Fonov S. "Luminescent Pressure Sensors in Aerodynamic Experiment", Moscow: TsAGI, CWA Int. Corp. 1997
8. Fonov S., Mosharov V., Radchenko V., Mihailov S. Kulesh V. "Application of the PSP for investigation of the oscillating pressure fields" AIAA Paper 98-2503, Presented at Appl. Aerodyn. Conf., 16th, Albuquerque, NM 1998.
9. Reda D.V. "Measurements of continuous pressure and shear distributions using coating and imaging techniques", AIAA Journal v.36, pp. 895-899, 1998.
10. Zhong, S. "Detection of flow separation and reattachment using shear-sensitive liquid crystals", Experiment in Fluids, v.32 pp.667-673, 2002
11. Tarasov V.N, Orlov A.A. "Method for determining shear stress on aerodynamic model surface", Patent of Russia, 4841553/23/1990
12. Tarasov V., S. Fonov, A. Morozov, "New gauges for direct skin friction measurements." Proc. Of 17th International Congress on Instrumentation in Aerospace Simulation Facilities (ICIASF), Monterey, California, 29 Sept to 2 Oct 1997.

13. Landau L.D, Lifshitz E.M. "Course of Theoretical Physics: Theory of Elasticity", Vol. 7 Butterworth-Heinemann, 1995, 260pp
14. Braess D. "Finite Element", Second Edition, Cambridge University Press, 2001